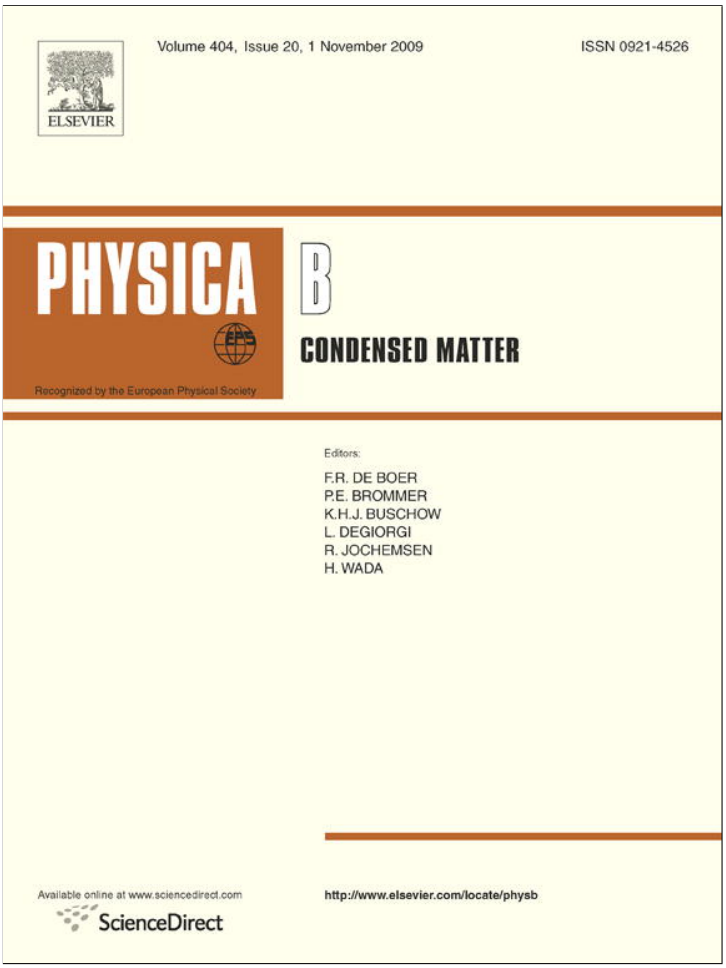

Physica B 404 (2009) 3519–3524

Contents lists available at ScienceDirect

Physica B

journal homepage: www.elsevier.com/locate/physb

Enhancement of electrical conductivity by Al-doped ZnO ceramic varistors

A. Sedky *, Ayman Al- Sawalha, A.M. Yassin

Physics Department, Faculty of Science, King Faisal University, Al-Hassa 31982, P.O. Box 400, Saudi Arabia

ARTICLE INFO

Article history:
Received 17 March 2009
Received in revised form
20 May 2009
Accepted 28 May 2009

Keywords:
Al doping
Wurtzite structure
Breakdown
Conductivity and Upturn region

ABSTRACT

$Zn_{1-x}Al_xO$ ceramic samples with various x values ($0.00 \le x \le 0.20$) are sintered in air at temperatures of 850 °C for 10 h and then quenched to room temperature. Structural, surface morphology and I–V characteristics of the samples are investigated using X-ray diffractometer (XRD), scanning electron microscope (SEM) and dc electrical measurements. It is found that addition of Al up to 0.05 does not influence the well-known peaks related to wurtzite structure of ZnO ceramics, and other unknown peaks could be formed above 0.05 of Al. The cell parameters of Al-doped samples are a little shorter than the undoped ZnO, and also the shape and size of grains are clearly affected. Average crystalline diameters, deduced from XRD analysis, are between 39.90 and 47.18 nm, which are 25 times lower than those obtained from SEM micrographs. Although breakdown field, nonlinear coefficient and barrier height are generally decreased by Al addition, the electrical conductivity is improved. These results are discussed in terms of the interaction mechanism between atoms of Al and Zn in both under and over-doped regions.

1. Introduction

Electrical conductivity of oxide semiconductors such as ZnO ceramic varistor depends on the amount and nature of oxygen vacancies that are generated during its synthesis [1,2]. These oxygen vacancies are normally controlled by several dopants added to ZnO such as Bi, Ni, Ga, Mn, Co, Sb, Al, Fe and Cr [3–7]. Therefore, it is very important to understand effects of these dopants on structural and nonlinear properties of this type of ZnO varistor. However, the effect of Al doping on the electrical properties of ZnO varistor has been investigated by several reports [8–11]. It has been observed that Al increased the current density in the upturn region and shifted its onset to lower fields, and consequently the grain conductivity of ZnO is increased. Since the conductivity in the upturn region depends on the grain conductivity of ZnO, a systematic study of the effect of Al doping on the conductivity of ZnO is, therefore, necessary.

With this purse in mind, a range of $Zn_{1-x}Al_xO$ ceramic samples with various x values are sintered in air at temperature of 850 °C for 10 h and then quenched from sintering temperature down to room temperature. Structural and grain morphology of the samples are investigated using X-ray diffractometer (XRD) and scanning electron microscope (SEM) techniques; while I–V characteristics are obtained using dc electrical measurements.

2. Experimental details

$Zn_{1-x}Al_xO$ samples with various x values ($0.00 \le x \le 0.20$) are synthesized using the conventional solid-state reaction method [7,12]. The powders of ZnO and Al_2O_3 (Aldrich 99.999 purity) are thoroughly mixed in required proportions and calcined at a temperature of 1000 °C in air for a period of 12 h. The resulting powders are ground, mixed, pressed into pellets and sintered at temperatures of 850 °C for 10 h in air. Finally, the samples are quenched from sintering temperature down to room temperature. The bulk density of the samples is measured in terms of their weight and volume. The phase purity and surface morphology of the samples are examined using X-ray diffractmeter and scanning electron microscope. I–V characteristics are obtained with an electrometer (model 6517, Keithley), 5 kV dc power supply and digital multimeter. The samples are well polished and sandwiched between two copper electrodes and the current is measured relative to the applied voltage. High-quality silver paint is used on the samples surfaces for electrical contact.

3. Results and discussion

It is noted that color of pure ZnO sample is white and it changed to yellow with Al addition. The bulk density of the samples, listed in Table 1, is generally decreased by Al. The structure of $Zn_{1-x}Al_xO$ samples, shown in Fig. 1(a), with $x \le 0.05$ is Wurtzite structure, and no additional peaks could be formed. When Al content is increased above 0.05, some of unidentified

* Corresponding author. Permanent address: Physics Department, Faculty of Science, Assiut University, Assiut, Egypt.
E-mail address: sedky1960@yahoo.com (A. Sedky).

0921-4526/$ - see front matter © 2009 Elsevier B.V. All rights reserved.
doi:10.1016/j.physb.2009.05.054

Table 1
ρ, D, a, c and average crystalline diameter versus Al content for Al-doped ZnO samples.

Al content	ρ (gm/cm^3)	D (SEM) (nm)	a (Å)	c (Å)	D_{100} (nm)	D_{002} (nm)	D_{111} (nm)	D_{102} (nm)	D_{110} (nm)	Average (nm)
0.00	6.35	1560	3.252	5.208	43.36	40.60	41.53	54.63	55.77	47.18
0.025	4.31	920	3.247	5.201	43.40	44.78	35.32	39.12	48.78	42.28
0.05	5.24	840	3.242	5.196	39.46	44.78	32.71	37.76	44.81	39.90
0.10	5.05	1020	3.231	5.188	36.11	37.22	38.36	49.68	55.84	43.44
0.20	4.31	1120	3.225	5.181	36.11	44.73	38.07	54.69	60.97	46.91

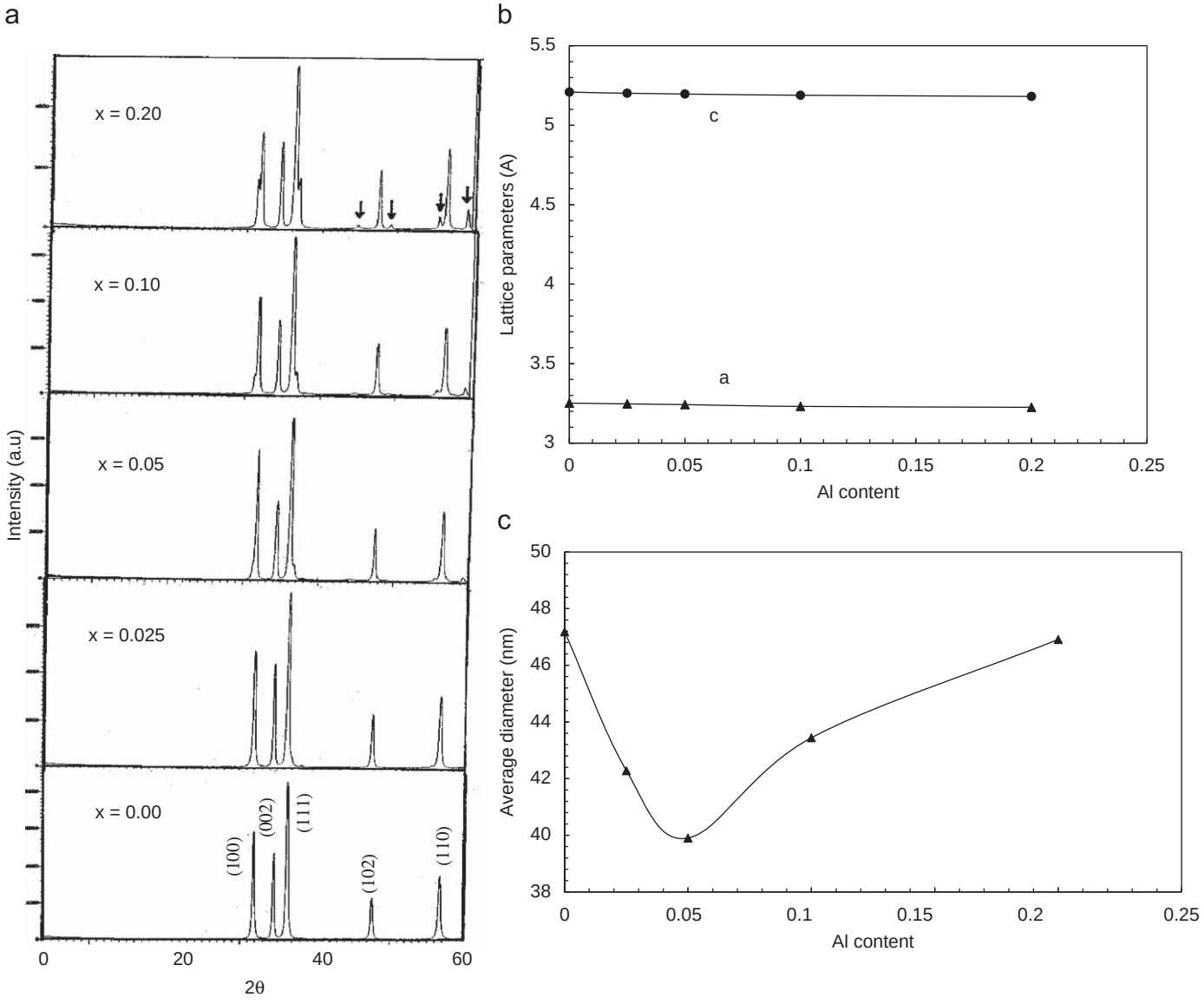

Fig. 1. (a) X-ray diffraction patterns of pure and Al-doped ZnO samples. (b) Lattice parameters of pure and Al-doped ZnO samples. (c) Average crystalline diameter deduced from XRD analysis of pure and Al-doped ZnO samples.

very low-intensity peaks denoted by arrowhead could be seen in the XRD pattern. This is because that with increasing Al content above 0.05, the solubility limit of Al through Zn lattice is reached, and some of Al atoms could be localized at the interstitial position. To further confirm that Al^{3+} has been substituted for Zn^{2+} in the unit cell, the lattice parameters of the samples are calculated and listed in Table 1. As shown in Fig. 1(b), the lattice parameters are decreased by Al addition, probably due the smaller ionic size of Al^{3+} (0.51 Å) than that of Zn^{2+} (0.74 Å). On the other hand, the average crystalline diameter D_{hkl} is evaluated in terms of X-ray line broadening described by the following Scherer's equation [13]:

$$D_{hkl} = \frac{k\lambda}{\Delta\theta \cos\theta} \quad (1)$$

where λ is X-ray wavelength ($\lambda = 1.5418$ Å), $\Delta\theta$ is half-maximum line width, θ is Bragg angle and K is constant ($K = 0.9$ for this type of ceramics). Average crystalline diameter versus Al content is shown in Fig. 1(c). Similar values are listed in Table 1. It is clear that values of D_{hkl} are decreased by Al addition up to 0.05,

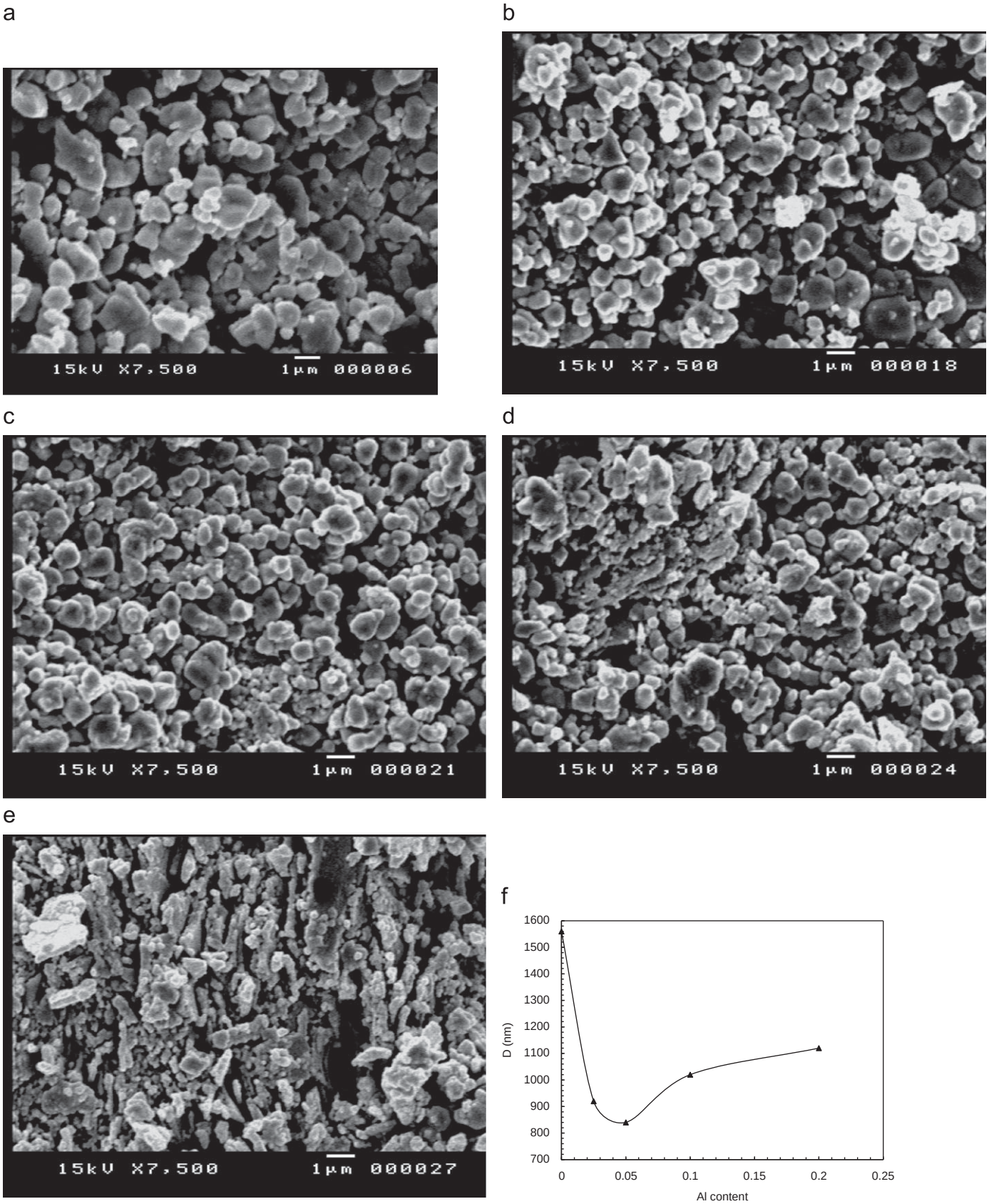

Fig. 2. (a) SEM photograph of pure ZnO varistor. (b) SEM photograph of 0.025 Al-doped ZnO varistor. (c) SEM photograph of 0.05 Al-doped ZnO varistor. (d) SEM photograph of 0.10 Al-doped ZnO varistor. (e) SEM photograph of 0.2 Al-doped ZnO varistor. (f) Grain size deduced from SEM micrograph of pure and Al-doped ZnO samples.

followed by an increase with further increase up to 0.20. The values of D_{hkl} are ranges between 39.90 and 47.18 nm for all samples.

The microstructures of pure and Al-doped ZnO samples are shown in Fig. 2(a)–(e). No second phases are formed at the grain boundaries, while Al decreased the average grain size as compared to ZnO sample. In ZnO sample, flake-type grains are absent, and there is a uniform granular precipitation on the mother grains. In 0.025 Al sample, the black regions are slightly increased and randomly distributed in the matrix structure. With increasing Al content up to 0.2, the flake shape grains appear with relatively small size and distributed randomly in the matrix structure, which may be responsible for the impurity phases as reported in the XRD pattern. The size of black regions is nearly unchanged, and the shape of grains became unclear. It is also apparent from Fig. 2(f) that average grain size, decreased with increasing Al addition up to 0.05, followed by an increase with further Al up to 0.20. Similar values are listed in Table 1. However, we obtained a typical behavior against Al content as compared to those obtained from XRD. But the average grains size of all samples are between 820 and 1560 nm, which are 25 times higher than those obtained from XRD analysis. However, it has been reported that diluted magnetic semiconductors are formed by partial substitution of n-type ZnO with small amount of magnetic transition metals such as Ni^{2+}. In $Zn_{0.95}Ni_{0.05}O$, TEM analysis indicates that most of the particles size is a round 60 nm [13]. This probably supports the average grain size deduced from XRD analysis rather than those obtained from normal SEM micrograph. The smaller ionic radii of Al^{3+} (0.51 Å) as compared to Ni^{2+} (0.69 Å) may be responsible for the difference of average grain size between Al and Ni samples. Anyhow, TEM or high-resolution SEM analysis will be taken into consideration for further research based on the considered samples.

There are three different regions observed in the *I–V* curves of the samples shown in Fig. 3(a). The first and third regions are nearly ohmic behavior, while the other is clearly nonlinear behavior (upturn region). However, the breakdown field E_B is usually taken as the field applied when the current density flowing through the varistor is 1 mA/cm^2 [7,14,15]. The variation of

Table 2
α, β and φ_B versus Al content for Al-doped ZnO samples.

A1 content	E_B (V/cm)	α_1	α_2	α_3	B (eV (cm V)$^{1/2}$)	Φ_B (eV)
0.00	694.44	1.82	31.15	2.38	3.2×10^{-14}	1.163
0.025	98	0.31	25.69	1.56	3.11×10^{-14}	1.118
0.05	12.5	0.30	21.01	1.39	8.41×10^{-14}	0.969
0.10	20.59	0.46	16.25	1.64	14×10^{-14}	1.111
0.20	128.21	1.33	20.79	1.92	4.12×10^{-14}	1.205

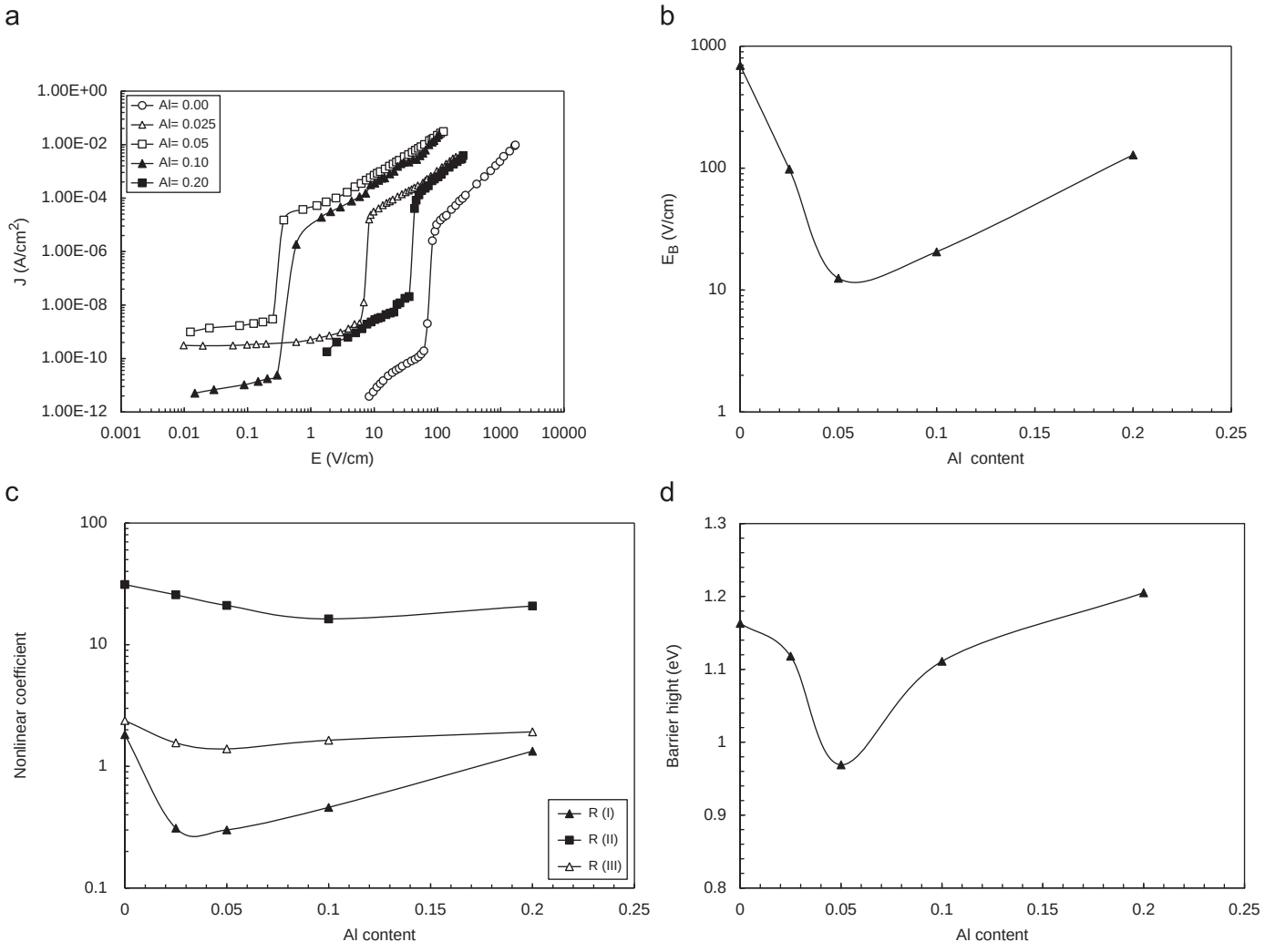

Fig. 3. (a) *I–V* characteristics for pure and Al-doped ZnO samples. (b) Breakdown field for pure and Al-doped ZnO samples. (c) Nonlinear coefficient for pure and Al-doped ZnO samples. (d) Barrier height for pure and Al-doped ZnO samples.

E_B against Al content is shown in Fig. 3(b). Similar values are listed in Table 2. It is clear that E_B is generally decreased by Al addition up to 0.05, followed by an increase with further Al up to 0.20. The values of E_B are ranges between 12.5 and 695 V/cm for all considered samples.

The current–voltage relation of a varistor is given by the following equation [14,15]:

$$J = (E/C)^{\alpha} \tag{2}$$

where J is the current density, E is the applied electric field, C is proportionality constant corresponding to the resistance of an ohmic resistor and α is the nonlinear coefficient. The current–voltage curves are plotted on a log–log scale, from which the slope of the curve gives the value of α [16]. The variation of α against Al content in the three different regions is shown in Fig. 3(c). Similar values are listed in Table 2. It is apparent that values of α are increased by 0.025 Al additions, followed by a decrease at 0.10, and then increased at 0.20. The values of α are between 16.25 and 31.15 for all samples. From these results, it is determined that the addition of low amount of Al^{3+} oxide to ZnO varistor composition decreased the non-ohmic features and shifted the breakdown fields to lower values.

Since Schottky-type grain boundary barriers exist in the present samples, the current density in the ohmic region of the varistor is related to the electric field by the following formula [7,17]:

$$J = AT^2 \exp[(\beta E^{1/2} - \varphi_B)/kT] \tag{3}$$

where A is the Richardson's constant $\{A = (4\rho emK^2/h^3)\}$, ρ is the varistor density, e is the electronic charge, m is the electronic mass, k is the Boltzmann constant, h is the Planks, constant, φ_B is the interface barrier height and β is a constant. By measuring the current density in the ohmic region and keeping the temperature constant, for two different values of applied fields, the values of φ_B and β can be easily obtained. The variation of φ_B against Al content shown in Fig. 3(d) indicates that φ_B decreased by Al addition up to 0.05, followed by an increase up to 0.20. This behavior is completely consistent with the behaviors of both nonlinear coefficient and breakdown field against Al content.

It is well known that electrical conductivity of ZnO samples at room temperature is controlled by the intrinsic defects generated at high temperature and also by the presence of dopants, either specifically added to the materials or not. In the present case, σ is calculated from the (J/E) curves in the first and third regions (ohmic regions). While, in the second region (nonlinear region), the current strongly increases due to the decrease of φ_B. Then, the conductivity in the nonlinear region is given by [18]

$$\sigma_2 = \sigma_1 \exp\left\{\frac{(\alpha - 1)(E_2 - E_1)}{E_2}\right\} \tag{4}$$

where σ_1 is the conductivity in the low field region (first region). E_1 and E_2 are the values of applied fields across the nonlinear region. For simplicity, the carrier mobility of 100 cm^2/Vs is taken at room temperature for the considered samples, irrespective of the sintering temperature or the chemical composition [19]. With this value, the density of carriers in the conduction band, n, can be easily calculated in terms of obtained values of electrical conductivity, $\sigma_{exp} = ne\mu$. Fig. 4 shows the dc electrical conductivity as a function of Al content in the three different regions. Similar values are listed in Table 3. It is clear that addition of Al generally enhanced the conductivity of ZnO in the three considered regions. Similar behavior is reported for electron density, see Table 3. The point to be noted shown in Fig. 4 is that σ decreased around an optimum value of Al content (0.05) as well as T_c versus carrier concentration in high T_c superconductors [20].

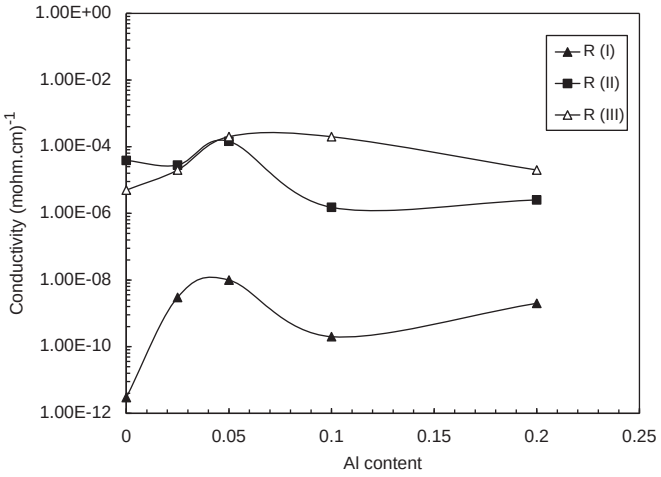

Fig. 4. Electrical conductivity for pure and Al-doped ZnO samples.

Table 3
Conductivity and electron density versus Al content in the three different regions for Al doped ZnO samples.

Al content	σ_1 $(\Omega cm)^{-1}$	n_1 (cm^{-3})	σ_2 $(\Omega cm)^{-1}$	n_2 (cm^{-3})	σ_3 $(\Omega cm)^{-1}$	n_3 (cm^{-3})
0.00	3.00E−12	1.88E+05	3.85E−05	2.41E+12	5.00E−06	3.13E+11
0.025	3.00E−9	1.88E+08	2.78E−05	1.74E+12	2.00E−05	1.25E+12
0.05	1.00E−08	6.25E+08	1.45E−04	9.06E+12	2.00E−04	1.25E+13
0.10	2.00E−10	1.25E+07	1.51E−06	9.44E+10	2.00E−04	1.25E+13
0.20	2.00E−9	1.25E+08	2.53E−06	1.58E+11	2.00E−05	1.25E+12

Therefore, there are two different regions around the optimum concentration of Al. The first is obtained below 0.05 and it is called under-doped region, while the other is obtained above 0.05 and it is called over-doped region.

To understand the mechanism of Al reaction with Zn in the ZnO structure, let us now discuss the expected reactions as follows:

Neutral Zn interstitial zinc atom ionized first as

$$Zn \rightarrow Zn^{+} + e, \text{ and secondly ionized as}$$

$$Zn^{+} \rightarrow +Zn^{++} + e$$

Such free electrons moves to the conduction band of ZnO and enhance the conductivity of ZnO. The conductivity of ZnO can be also increased by extrinsic defects at Zn site such as Al^{3+}. In Zn^{2+} substitute with Al^{3+}, some of free electrons are released and raise the conductivity of ZnO through increasing the electron density n.

Therefore, the interaction mechanism between Al and Zn will be as follows:

$$\frac{1}{2}Al_2O_3 \rightarrow \frac{1}{4}O_2 + Al^{Z} + e + ZnO \tag{5}$$

Al^{Z} is the ionized Al atom in Zn atom substitution site since Al acts as a donor. So, Al^{3+} goes to Zn sites and some additional free electrons are released. This reaction is consistent with the behavior of conductivity in the under-doped region ($Al \leq 0.05$). With increasing Al addition above 0.05, Al^{3+} can enter the structure and prefer interstitial sites of Zn sites and then moving to the interstitial position. At interstitial position, Al can follow the following reaction and absorbs an electron [15,21]:

$$\frac{1}{2}Al_2O_3 \rightarrow \frac{3}{4}O_2 + Al^{*} + P \tag{6}$$

where Al^{*} is the ionized Al atom in interstitial sites and P is the charge of positive hole. In this case, the Al behaves as

an acceptor, dominates the donor effect and decreases the conductivity. This reaction agrees very well with the conductivity behavior in the over-doped region ($Al > 0.05$), in agreement with the extra lines observed in the XRD patterns.

Anyhow, the normal state conductivity $\sigma_{300} \propto n\tau$, where n is carrier concentration and τ is relaxation time. So, Al doping primarily has two different effects; the first is the increase of electron density and the other is the decrease of τ due to structural distortion induced by the doping [22]. In the under-doped region, structural distortion is weak and the change of τ is ignorable. So, increasing n improved conductivity. However, in the over-doped region, structural distortion becomes strong and τ decreases markedly. As a result, conductivity is decreased, but still higher than undoped ZnO sample.

4. Conclusion

Structural and electrical properties of $Zn_{1-x}Al_xO$ ceramic samples are well investigated. It is found that Al does not influence the well-known peaks related to wurtzite structure of ZnO ceramics, and other unknown peaks could be formed with further Al addition. Furthermore, average crystalline diameters, deduced from XRD analysis, are between 39.90 and 47.18 nm, which are 25 times lower than those obtained from SEM micrographs. Although, addition of Al generally decreased break-down field, barrier height nonlinear coefficient and barrier height, the electrical conductivity is improved. The electron density and structural distortion, produced by Al doping in both under and over-doped regions, are found to be the main factors responsible for the present behavior.

Acknowledgments

The authors would like to thank the Deanship of Scientific Research, King Faisal University for providing facilities and maintenance support during the present work (No: 90069).

References

[1] J.M. Madou, R.S. Morrison, Chemical Sensing with Solid State Devices, Academic Press, San Diego, CA, 1989 (Chapters 2, 3 and 12).
[2] P. Bonasewicz, W. hirscawald, G. Newnann, Phys. Status Solidi (a) 97 (1986) 593.
[3] R.D. Clark, J. Am. Ceram. Soc. 82 (1999) 485.
[4] Q.P. Mantas, L.J. Baptista, J. Eur. Ceram. Soc. 15 (1995) 605.
[5] Q.P. Mantas, L.J. Baptista, J. Electroceram. 4 (2000) 215.
[6] Q.P. Mantas, L.J. Baptista, R.J. Frade, In: K. Kuomoto, L.M. Sheppard, H. Matsubara (Eds.), Ceramic Transactions, vol. 21, Am. Ceram. Soc., OH, 1996, p. 61.
[7] A. Sedky, M. Abu-Abdeen, Abdul-Aziz A. Almulhem, Physica B 388 (2007) 266.
[8] G.W. Clarson, K.T. Gupta, J. Appl. Phys. 53 (1982) 5746.
[9] L.Y. Tsal, L.C. Huang, C.C. Wei, J. Mater. Sci. Lett. 4 (1985) 1305.
[10] Jiaping Han, P.Q. Mantas, A.M.R. Senos, J. Eur. Ceram. Soc. 21 (2001) 1883.
[11] J. Han, Q.P. Mantas, A.M.R. Senos, P.Q. Mantas, J. Mater. Res. 16 (2001) 459.
[12] M.S. Castro, C.M. Aldao, J. Eur. Ceram. Soc. 19 (1998) 511.
[13] Guangqing Pei, Changtai Xia, Shixun Cao, Jungang Zhang, Feng Wu, Jun Xu, JMMM 302 (2) (2006) 340.
[14] V.V. Deshpande, M.M. Patil, V. Ravi, Ceram. Int. 32 (2006) 85.
[15] Mourad Houabes, Slavko Bernik, Chabance Talhi, Ai Bui, Ceram. Int. 29 (6) (2005) 783.
[16] M. Matsuoka, Jpn. J. Appl. Phys. 10 (6) (1971) 736.
[17] S.R. Dhage, Vandana Choube, V. Ravi, Mater. Sci. Eng. B 110 (2004) 168.
[18] A. Sedky, Unpublished.
[19] J. Han, P.Q. Mantas, A.M.R. Senos, J. Eur. Ceram. Soc. 22 (2002) 49.
[20] J.M. Tarascon, L.H. Greene, W.R. Mckinnan, G.W. Hall, T. Geballe, Science 235 (1987) 1373.
[21] T.K. Gupta, J. Mater. Res. 7 (12) (1992) 3280.
[22] A. Sedky, Abdalaziz A. Almulhem, Sobhy S. Ibrahim, Smart Mater. Struct. 15 (2006) N99.